Progress in Organic Coatings 103 (2017) 40–47

Contents lists available at ScienceDirect

Progress in Organic Coatings

journal homepage: www.elsevier.com/locate/porgcoat

Electrochemical and *in vitro* bioactivity of nanocomposite gelatin-forsterite coatings on AISI 316 L stainless steel

R. Torkaman [1], S. Darvishi [1], M. Jokar, M. Kharaziha *, M Karbasi

Department of Materials Engineering, Isfahan University of Technology, Isfahan 84156-83111, Iran

ARTICLE INFO

Article history:
Received 28 June 2016
Accepted 25 November 2016

Keywords:
Gelatin
Forsterite
Nanocomposite coating
AISI 316L stainless steel
Corrosion resistance
In vitro bioactivity

ABSTRACT

AISI 316L stainless steel has been widely considered as implant materials in biomedical applications owing to its low cost and superior strength. However, its weak corrosion resistance due to the release of nickel, chromate and molybdenum ions as well as its inert nature limits its clinical application specifically long-standing performances. The aim of this study was to prepare and characterize gelatin-forsterite (Mg_2SiO_4) nanocomposite coatings consisting of various amounts of forsterite nanopowder (0, 1, 2.5 and 5 wt.%) on AISI 316L substrate in order to improve simultaneously corrosion resistance and *in vitro* bioactivity. Nanocomposite gelatin-forsterite coatings were characterized by Fourier transform infrared spectroscopy, scanning electron microscopy and X-ray diffraction. Furthermore, the bioactivity of gelatin-forsterite coated specimens were evaluated via soaking in simulated body fluid (SBF) for 28 days at 37 °C. Results demonstrated the formation of crack-free and homogeneous coatings without any observable defect and pore. The surface roughness and adhesion strength of the coatings enhanced with increasing forsterite content. Moreover, the corrosion evaluation considered by potentiodynamic polarization and electrochemical impedance spectroscopy (EIS) demonstrated that compered to unmodified AISI 316L substrate, the corrosion resistance of gelatin-forsterite nanocomposite-coated substrates significantly improved. Moreover, nanocomposite coatings were able to persist severe localized corrosion in physiological solution indicating their long-term biostability. Moreover, the formation of bone-like apatite layer on the nanocomposite-coated samples was observed in SBF, which might be helpful to integrate with host tissue. Overall, it is anticipated that the novel proposed nanocomposite coatings of gelatin-forsterite might be potentially useful for orthopedic implants.

1. Introduction

AISI 316L stainless steel has been widely applied in medical fields especially as temporary implants owning to its low cost and superior strength [1]. However, AISI 316L has some drawbacks consisting of poor wear resistance to common forms of wear and contact damage [2,3], inability to form directly chemical bonds to natural bone tissue [3] as well as weak resistance to release metal ions such as nickel, chromate and molybdenum leading to less biocompatibility and long-standing performance [4,5]. In order to improve the corrosion resistance and stimulate the bone in growth to AISI 316L implant surface, various surface modification strategies consisting of mechanical and electrochemical polishing [6], thermal treatment [7], ion implantation [8] and alkali and heat-treatment [9] as well as several ceramic (e.g. calcium phosphate-based material such as hydroxyapatite (HA) [10–12]), polymer (e.g. poly(ε-caprolactone) (PCL) [13]) and composite [14,15] coatings have been employed. Between these approaches, composite coatings could simultaneously improve corrosion resistance and bioactivity via the chemical and physical bonding with host tissues making them perfect option for orthopedic implants [16,17]. Compared to pure ceramic coatings, composite coatings revealed reduced brittleness and crack formation providing improved corrosion resistance [18]. Various kinds of bioactive ceramics have been introduced to develop composite coating on metallic substrates consisting of HA [17,18], TiO_2/ZrO_2 [19] and bioactive glass [20] embedded natural and synthetic polymers such as PCL [21] and chitosan [17,22].

Forsterite with chemical formula Mg_2SiO_4 has recently been introduced as a biocompatible and bioactive ceramic with better mechanical properties compared to HA and bioactive glass [23–25]. Results demonstrated that Mg and Si ions could release during soaking in biological environment which stimulate bone in

* Corresponding author.
E-mail address: ma.kharaziha@gmail.com (M. Kharaziha).
[1] These authors equally contributed to this work.

http://dx.doi.org/10.1016/j.porgcoat.2016.11.029
0300-9440/

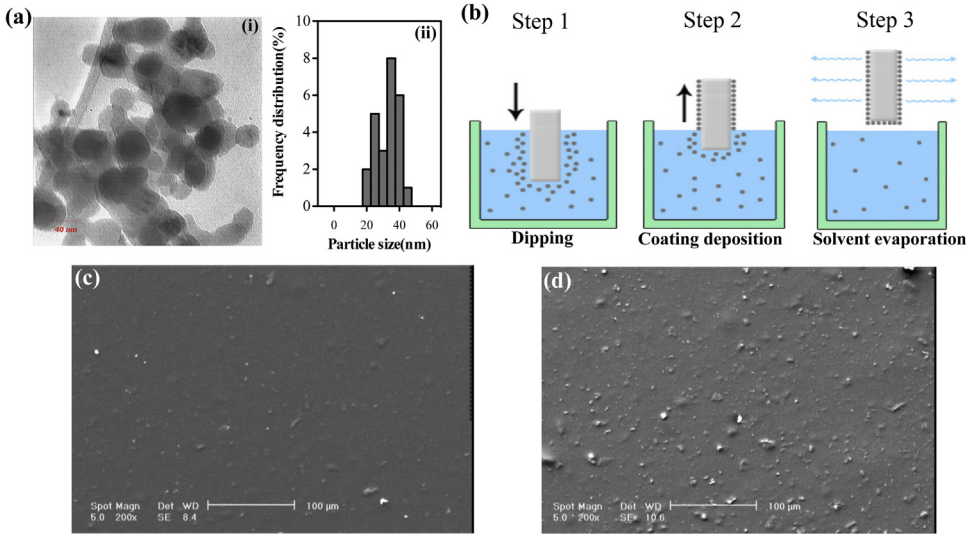

Fig. 1. (a) TEM micrograph (i) and the frequency histogram of particle size (ii) of forsterite nanopowder, (b) The schematic of dip coating process consisting of: step 1) dipping of the substrate into the suspension, step 2) formation of wet layer by withdrawing the substrate, step 3) gelation of the layer by solvent evaporation. SEM image of G-1F coated samples with dipping period of (c) 3 times and (d) 5 times.

growth and regeneration [26]. Forsterite has been widely applied as coatings on various kinds of ceramics and metallic scaffolds and implants [27–30]. Results demonstrated that the incorporation of forsterite nanopowder in the coatings could significantly improve their mechanical properties such as elastic modulus, hardness and fracture toughness as well as corrosion resistance [29]. In other words, gelatin is a natural polymer derived from collagen through an acid (type A-gelatin) or alkali (type B-gelatin) hydrolysis. Thanks to its similarity to the natural bone, relatively low cost, desirable encouragement to bone regeneration and good adhesiveness and hemostatic properties, gelatin has been widely used in tissue engineering [31,32], pharmaceutical applications [33] as well as food and cosmetic products [34]. Moreover, gelatin has recently been applied as coatings on various kinds of implants and revealed the formation of homogeneous and well-adherent coating [35,36]. However, according to our knowledge, the limited studies have focused on the nanocomposite coatings based on gelatin protein. In addition, the bioactivity and corrosion resistance of gelatin based composite coatings have not evaluated yet.

The aim of this study was to prepare nanocomposite coatings consisting of gelatin and various amounts of forsterite nanopowder on AISI 316L substrate using dip coating process. Moreover, the effects of forsterite nanopowder concentrations on the coating roughness, adhesion and morphology were studied. Finally, the bioactivity and corrosion resistance of nanocomposite-coated substrates were evaluated.

2. Materials and methods

2.1. Synthesis of forsterite nanopowder

Forsterite nanopowder with spherical particles (Fig. 1(a–i)) and particle size of 25–45 nm (Fig. 1(a–ii)) was synthesized according to the sol-gel process based on our previous report [37]. Briefly, after preparation of magnesium nitrate hexahydrate ($(Mg(NO_3)_2{\cdot}6H_2O)$, Merck) aqueous solution, colloidal silica (SiO_2, 34 wt.% solid fraction, Sigma) was added to it in order to provide Mg: Si mole ratio = 2:1. Meanwhile, aqueous solution of sucrose (sucrose-to-metal mole ratio = 4:1, Merck, 99.9% purity) was separately prepared and polyvinyl alcohol (PVA) aqueous solution was added to it (PVA monomer-to-metal molar ratio = 0.8:1, Merck). The amount of sucrose, PVA and sucrose-to-metal mole ratio were selected based on the previous reports [37,38]. As prepared PVA-sucrose solution was added to Mg-Si solution and pH was adjusted to 1 using nitric acid. PVA and sucrose were applied in the forsterite synthesize procedure due to the different hydrolysis and condensation rates of silica and alkoxides leading to chemical inhomogeneity of the gels and, therefore, unwanted phases. In this process, nitric acid could break sucrose into glucose and fructose. Decomposed products consisted of —OH and —COOH groups which could encourage the binding of Mg^{2+} ions in the homogeneous solution. In other words, PVA could develop polymeric network which could trap colloidal silica nanoparticles leading to their homogenous distribution [38]. After continuous stirring at 90 °C for 2 h, the solution was preserved at room temperature overnight, dried at 200 °C and finally calcined at 900 °C for 2 h.

2.2. Preparation of AISI 316L stainless steel substrates

AISI 316L samples cut into square specimens having dimensions of $10 \times 10 \times 2\,mm^3$ were applied as substrates. Prior to the coating process, the substrates were mechanically polished using SiC papers with the grit sizes of 80, 120, 240, 320, 600, 800, 1200 and 2000, sequentially, and rinsed with deionized (DI) water. Afterwards, in order to better attachment of coatings to the substrates, they were immersed in solution consisting of 30:70 vol ratio of H_2O_2: HNO_3 for 30 s. Consequently, as prepared substrates were ultrasonically cleaned in acetone to remove residual grease and, then, DI water for 1 h in order to remove surface impurities. Finally, the AISI 316L substrates were air dried at 60 °C overnight.

2.3. Fabrication of gelatin-forsterite coatings

Before coating process, nanocomposite suspensions containing gelatin with different amounts of forsterite nanopowder were prepared. Initially, 8 wt.% gelatin (type A porcine skin, Mw = 50,000–100,000, Sigma) solution in 20 wt.% acetic acid was prepared at room temperature. After complete gelatin dissolution, various amounts of forsterite nanopowder (0, 1, 3, and 5 wt.%) were added to it. To provide uniform dispersion of forsterite nanopowder, the suspensions were magnetically stirred for 24 h at room temperature. Based on the amounts of forsterite nanopowder (0, 1, 3 and 5 wt.%), the suspensions and the final coatings were named as Gelatin, G-1F, G-3F and G-5F, respectively. Since gelatin is water

soluble, crosslinking is required to stabilize its structure. In this research, 1-ethyl-3-(3-dimethylaminopropyl) carbodiimide (EDC, Sigma) which is less cytotoxic compared to other crosslinkers such as glutaraldehyde was used to chemically crosslink gelatin. In this regards, 9 wt.% EDC solution in ethanol was added to the suspensions and stirred for 24 h at 50 °C. Before coating process, the suspensions were sonicated for 1 h at room temperature to prevent from forsterite nanopowder agglomeration. It is worth noting that, the concentration of EDC and the stirring time before coating process was optimized according to the preliminary experiments on the various concentrations of EDC solution (5, 7, 9 and 12 wt.%) and stirring times (2, 12 and 24 h) based on the visual evaluation of the coatings.

Dip coating process was applied to develop nanocomposite coatings, based on Fig. 1(b). This process consisted of three stages: immersion of the substrates, deposition of the suspension and the evaporation of the solvent. In this process, the substrates were initially dipped in the sonicated gelatin-forsterite suspensions at a constant rate (5 mm/min (first step)). The samples were remained in the suspensions for 1 min in order to deposit a thin layer of suspensions on the substrates while there were pulled up. The samples were withdrawn at a fixed speed of 5 mm/min to provide uniform thickness of the coatings on the substrates (second step). The samples were kept at room temperature for 5 min in order to solvent evaporation (third step). In order to develop a uniform and dense gelatin-forsterite coating, these processes was performed three and five times, continuously, in order to evaluate the optimized process.

2.4. Characterization of the nanocomposite coated substrates

The surface morphology of the coated samples was investigated by scanning electron microscopy (SEM, S360, Cambridge). Before SEM imaging, the samples were gold-coated using sputter coater (SCD 005). Fourier transform infrared spectroscopy (FTIR, Bomem, MB-100) was applied in the range 600–4000 cm^{-1} to determine the characteristic bonds of forsterite and gelatin. The phase identification of coated substrates was performed using X-ray diffraction (XRD, Philips X'Pert-MPD system) using monochromatized CuKα radiation.

As the performance of coatings directly depended on the mechanical integrity of coating-substrate systems, the adhesion of coatings to the substrates was estimated to determine the durability and longevity of the whole system. Adhesion is a surface phenomenon which is related to the physical forces and chemical interactions at the interface of coatings and substrates. Various techniques have been applied to examine the adhesion strength of coatings [39]. In this research, the adhesion strength between the gelatin-forsterite layers and substrates was determined according to the American Society of Testing and Materials (ASTM) test protocol D 3359 using PAT-2000 adhesion test kit (Paul N. Gardner Co., Pompano Beach, FL). This process consisted of applying and then removing pressure-sensitive tape over 25 squares made on the coating and the determination of the parts removed from the surface of samples. At the end of this test, the number of the parts removed from the surface was measured visually and the adhesion of coatings was rated on the scale of 0–5B. While "5B" referred to the best coating strength in which the edges of the cuts were completely smooth and none of the squares of the lattice was detached, scale "0" revealed the worst strength between coating and substrates. Surface roughness of the gelatin-forsterite samples was measured by a laser surface profilometer (Perthometer PGK 120, Mahr GmbH, Göttingen, Germany). Moreover, the thickness of the coatings was estimated using a coating thickness gauge. At least ten thickness measurements were taken from the various positions on the coatings and the average thickness with standard deviation was reported.

In vitro bioactivity of the coated substrates was evaluated by immersing in simulated body fluid (SBF) for 7, 14 and 28 days. The SBF solution was prepared based on Kokubo et al. protocol [40] and the samples were immersed in SBF solution for 28 days at 37 °C. Meanwhile, the pH of solution was recorded at the determined times and the formation of the apatite layer on the samples surfaces was evaluated by SEM imaging. The formation of apatite layer on the surface of membranes was demonstrated using SEM coupled with Energy-Dispersive Spectroscopy (EDS).

Electrochemical measurements were conducted using a conventional three-electrode electrochemical cell with the samples as the working electrodes, a platinum plate as the auxiliary electrode and a saturated calomel electrode (SCE) as the reference. Electrochemical tests were carried out using a PARSTAT2273 (Priceton Applied Research). The corrosion test was conducted in standard buffer phosphate saline (PBS) at pH = 7.4. The corrosion resistance of samples was tested by means of potentiodynamic polarization curves and electrochemical impedance spectroscopy (EIS). Prior to polarization, the samples were immersed in PBS for 1 h. The polarization scan was 250 mV vs open circuit polarization test (OCP) at the scan rate of 1 mV/s. For EIS measurement, the perturbation amplitude was 10 mV and the frequency range was from 10^5 Hz to 10^{-3} Hz.

2.5. Statistical analysis

All the data were presented in mean ± standard deviation (SD) and statistical significance was measured by performing one-way ANOVA analysis followed by Tukey's multiple comparison using GraphPad, Prism Software (V.5). Differences were taken to be significant for $P < 0.05$.

3. Result and discussion

3.1. Structural and chemical characterization of gelatin-forsterite coating

The thickness, densification and the amount of forsterite nanopowder deposited on the substrates basically depended on the number of dipping process [41]. SEM images of G-5F coated samples after dipping process repeated for 3 and 5 times (Fig. 1(c) and (d)) demonstrated that 5-dip coated sample had a densely packed coated morphology consisting of further forsterite nanoparticles which homogenously dispersed within the gelatin matrix. Hence, 5-time dipping was selected for the coating of the substrates and further study. The SEM images of the coated samples consisting of various amounts of forsterite nanopowder confirmed the formation of crack-free coatings without any defect representing the addition of forsterite nanopowder did not considerably alternate the dense and homogenous nature of gelatin coating (Fig. 2). While pure gelatin coating consisted of smooth and uniform morphology, nanocomposite coated samples consisting of two phases of forsterite nanopowder distributed within smooth gelatin matrix. Increasing forsterite nanopowder from 1 to 5 wt.% led to enhancement amount of forsterite nanopowder within the coatings. Moreover, the agglomeration of forsterite nanopowder (indicated by circle) could be observed at G-5F coated sample which could be due to the high concentration of nanoparticles in the suspensions. Table 1 shows the thickness of coatings determined using the coating thickness gauge. The estimated thickness was similarly reported for other coatings prepared using dip coating technique [42]. Moreover, results demonstrated that there was no significant difference between the thicknesses of various coatings ($P > 0.05$).

FTIR spectra of forsterite nanopowder as well as gelatin and G-5F coated samples demonstrated the presence of gelatin and

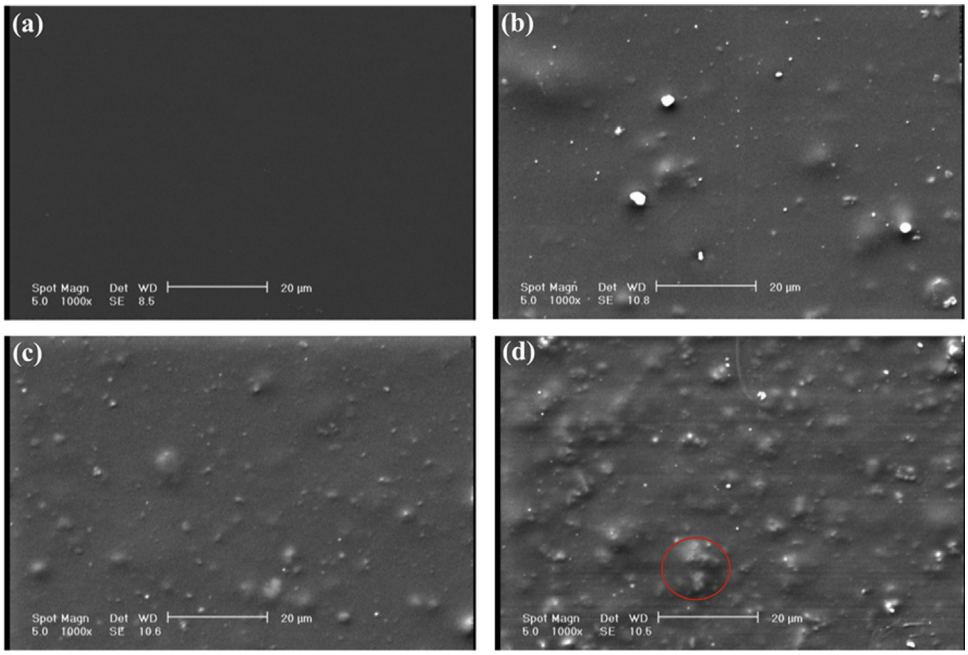

Fig. 2. SEM images of (a) pure gelatine, (b) G-1F, (c) G-3F and (d) G-5F nanocomposite coated samples. The circle indicates agglomeration of forsterite nanopowder.

Table 1
Surface roughness, thickness and adhesion of coatings deposited on the 316L substrates (*, +: Compared to Gelatin and G-1F coated substrates, respectively. ($P < 0.05$)).

Sample	Thickness of coating (μm)	Roughness (Ra) (μm)	Classification of cross-cut tape test	Percent area removed in cross-cut tape test
Gelatin	2.14 ± 0.9	0.356 ± 0.12	2B	15%
G-1F	2.82 ± 1.1	1.199 ± 0.03*	3B	10%
G-3F	3.20 ± 1.8	1.447 ± 0.06*	3B	5%
G-5F	3.52 ± 2.7	2.210 ± 0.1*+	4B	Less than 5%

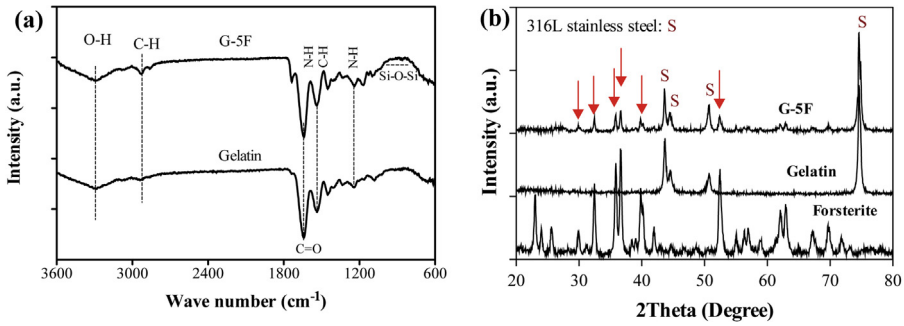

Fig. 3. (a) FTIR spectra and (b) XRD patterns of Gelatin and G-5F coated AISI 316L substrate. XRD pattern of pure forsterite nanopowder was also inserted as control. The arrows indicate the characteristic peaks of forsterite presented in G-5F coating.

forsterite nanopowder within coatings (Fig. 3(a)). G-5F coated sample consisted of the characteristic peaks of gelatin at 1650 cm^{-1} (C=O stretching), 1550 cm^{-1} (N—H bend and C—H stretching), 1267 cm^{-1} (N—H stretching) and 3300 cm^{-1} (N—H stretching vibration), attributed to amide I, amide II, amide III and amide A peak, respectively. Furthermore, the characteristic absorption bands of forsterite at 830–1000 cm^{-1} corresponded to the various vibration modes of Si—O—Si bonds were observed [43,44].

XRD analysis was applied in order to confirm the presence of gelatin and forsterite nanopowder within the coatings (Fig. 3(b)). According to the standard card of forsterite (JCDP# 34–0189), XRD pattern of forsterite nanopowder demonstrated the formation of pure and well-crystalline forsterite nanopowder without any impurity. XRD pattern of gelatin coated sample comprised of AISI 316L characteristic peaks. Based on XRD patterns, AISI 316L substrate consisted of face centered cubic (FCC) γ-austenitic phase with characteristic peaks at $2\theta = 44.1$ and 51.4 and assigned to (111) and (200) planes, respectively (JCDP# 33-0945) as well as body centered cubic (BCC) α-ferrite phase with the characteristic peak located at $2\theta = 44.7^\circ$ ((110) planes) (JCDP# 06-0696) [45]. Gelatin with amorphous nature did not have any intensify peak in XRD pattern except a broad peak between 15° and 25 ° [46,47]. XRD pattern of G-5F coated sample consisted of the main characteristic peaks of forsterite at $2\theta = 20.9$, 35.8, 36.7, 41.07 and 52.7° proving the presence of forsterite nanopowder in this coating. Moreover, the intensity of the AISI 316L peaks reduced in the XRD pattern of G-5F sample which might be due to the presence of crystalline forsterite nanopowder with sharp peaks. Furthermore, compared to the XRD pattern of the pure gelatin coated sample, the intensity of broad gelatin peak reduced in the G-5F coated sample which might be due to reducing gelatin percentage in the nanocomposite coated sample [48].

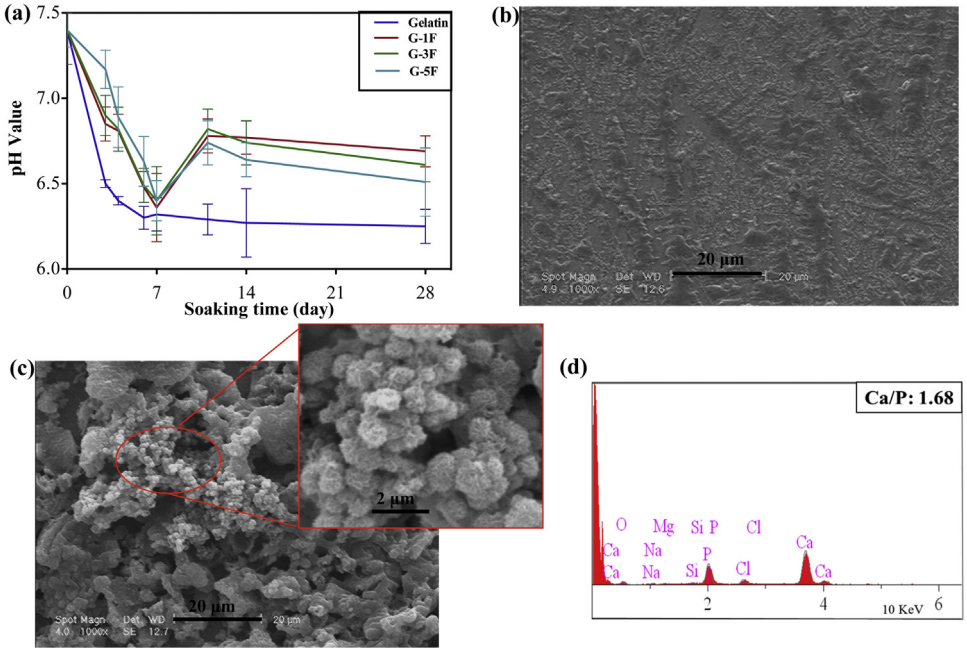

Fig. 4. (a) pH changes of SBF solution during the immersion of coated samples.SEM images of (b) Gelatin and (c) G-5F coated samples after 28 days soaking in SBF. (d) EDS spectrum of the G-5F coated sample after 28 days soaking in SBF.

The roughness of implant surface affects the osteoblast responses at the cell-surface interfaces and consequently the formation of chemical binding with host tissue [49–51]. The measured surface roughness (Ra) of coated samples demonstrated the remarkably effects of forsterite nanopowder on the surface roughness (Table 1). Incorporation of forsterite nanopowder upon 5 wt.% (G-5F) resulted in considerably enhanced surface roughness from 0.356 ± 0.12 μm (for gelatin coated sample) to 2.210 ± 0.1 μm ($P < 0.05$). It was likely due to the distribution of fine forsterite nanopowder in the matrix, leading to the enhanced surface inhomogeneity. The roughness of coated samples significantly affected the adhesion between coating layer and substrate (Table 1). While all nanocomposite coatings revealed fine adhesion strength with its substrate, it was noticeably improved with increasing amount of forsterite nanopowder. The addition of forsterite nanopowder from 0 wt.% to 5 wt.% promoted coating adhesion from 2 B to 4 B according to ASTM D 3359. It might be due to increasing surface roughness in these samples and consequently increasing the substrate interfaces with its coating [52].

3.2. In vitro *bioactivity assessment*

In vitro bioactivity is a crucial factor to determine bone growth directly onto the implant surfaces (osseointegration) preventing from loosening without infection (aseptic loosening) [53]. Since AISI 316L implants lack a biologically active surface, various kinds of bioactive coatings have been developed to supplement the function of these implants [54,55,56]. Bioactive coatings should be osteoconductive to stimulate osteoblasts attachment, proliferation and growth on the surface of the implant in order to form a confidant bone-implant bonding [57].

In vitro bioactivity of coated samples was considered with respect to bone-like apatite formation on the surface of samples by incubation in SBF solution. pH changes of SBF solution after soaking of various coated samples was depicted in Fig. 4(a). During the first week of soaking, a gradual decrease in pH value of SBF solution could be observed in all samples originating from acidic products of gelatin degradation. In the second period (7–14 days), while the gradual decrease in pH value of SBF solution could still be seen during the soaking of the gelatin coated samples, the increase in pH value was detected in all nanocomposite coated samples. These trends were similarly reported in other reports on the silicate based ceramics and could be due to the release of magnesium ions in SBF solution leading to the formation of negatively charged groups of silanol (—Si—OH) on the surface of samples. Silanol group formation could contribute in the nucleation of Ca-P in a uniform manner with prolonged soaking time [58–61]. Ca-P nucleation afforded the positively charged positions for the attraction of phosphate and carbonates groups in SBF and resulted in the formation of a phosphate layer [37]. Due to the deposition of Ca and P ions on the surface and creation of carbonate hydroxyapatite, prolonged soaking time (>14 days) resulted in slightly reduce in pH values of SBF solution depending on the forsterite content.

SEM images as well as EDS analysis could confirm pH changes of SBF solution. Fig. 4(b) and (c) shows the SEM images of pure gelatin and G-5F coated samples after 28 days of soaking in SBF solution, respectively. Compared to pure gelatin coated sample (Fig. 4(b)), the surface morphology of G-5F coated one (Fig. 4(c)) dramatically changed. According to the high magnification SEM image of G-5F coated sample, spherical-like particles with size of 300–400 nm were uniformly covered the surface of G-5F coated sample. According to the EDS analyses (Fig. 4(d)), these nanoparticles contained Ca and P ions accumulated from SBF solution on the coating. Moreover, Ca/P ratio of deposition was about 1.68, which was close to 1.67 of bone-like apatite. These results recommended that the incorporation of forsterite into gelatin matrix could stimulate the apatite formation ability which may be beneficial to direct bone-bonding *in vivo* [62,63].

3.3. *Electrochemical corrosion evaluation*

The corrosion resistivity of gelatin and gelatin-forsterite coated as well as uncoated AISI 316L samples was evaluated using potentiodynamic polarization analysis in PBS solution at room temperature and the electrochemical polarization curves were assessed (Fig. 5). The polarization parameters consisting of the corrosion

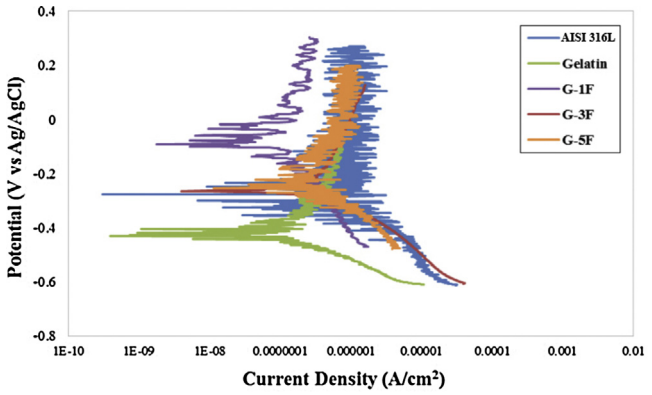

Fig. 5. Potentiodynamic polarization curves of uncoated as well as gelatin and gelatin-forsterite nanocomposite coated samples in PBS at pH = 7.4.

Table 2
The analysis data extracted from Potentiodynamic polarization curves (Fig. 5).

Sample	Current density (A/cm^2)	Potential (V)
AISI 316L	7.03E-7	−0.28
Gelatin	4.26E-7	−0.43
G-1F	1.59E-8	−0.09
G-3F	1.61E-7	−0.25
G-5F	3.07E-7	−0.26

potential (E_{corr}) and corrosion current density (I_{corr}) extracted from the graphs, are presented in Table 2. Generally, coated samples revealed less corrosion current density than uncoated AISI 316L demonstrating enhanced corrosion resistance. It could be due to the reduction of electron transfer provided by coatings. In addition, the incorporation of forsterite nanopowder resulted in shifting the corrosion potential (E_{corr}) to more positive potential (Table 2). Moreover, the corrosion density (I_{corr}) of the nanocomposite coated samples, especially G-1F coated one ($1.59 \times E^{-8}$ A/cm^2) significantly reduced compared to gelatin coated one ($7.03 \times E^{-7}$ A/cm^2) confirming the crucial role of gelatin-forsterite coatings to improve the corrosion resistivity of AISI 316L. This behavior might be due to the formation of more compact and thin layer of nanocomposite coating compared to the oxide film on the uncoated AISI 316L. The oxide film layer was not stable enough in the solution and, hence, could not sufficiently protect against pitting corrosion. Moreover, according to the other nanocomposite-coated samples, it might be due to the corrosion protection role of these coatings against electron and ions diffusion, which decreased the electrochemical reactions at the interface of AISI 316L and electrolyte solution [3,36]. In other words, the gelatin-forsterite coated samples could properly perform the desirable task of decreasing the corrosion rate of the 316LSS substrate. However, the incorporation of forsterite nanopowder upon 1 wt.% resulted in reduced corrosion resistance compared to G-1F coated sample. It might be due to the agglomeration of forsterite nanoparticles and formation of irregularly shaped nanostructured topographies leading to the enhanced surface roughness. Surface roughness revealed the effective role on the superior corrosion rate of nanocomposite coatings. According to the previous investigations, greater surface roughness could reduce electron work function (EWF) and increase local EWF fluctuation leading to lower pitting potential (the potential at which metastable pits start to form on the surface) [64,65]. Such fluctuation could stimulate the formation of microelectrodes and, consequently, accelerate corrosion [65]. Based on our results, G-1F coated sample revealed the best corrosion behavior compared to other samples.

EIS analysis was also performed on the uncoated AISI 316L as well as gelatin and gelatin-forsterite nanocomposite coated samples and the Nyquist and Bode plots were evaluated (Fig. 6). Nyquist diagram of uncoated 316LSS as well as gelatin and gelatin-forsterite nanocomposite coated samples (Fig. 6(a)) revealed only one capacitance loop attributed to the protective characteristics of the coatings. This behavior was similarly reported by Xu et al. [36] who worked on the gelatin/nanoparticles coated magnesium substrate. All coated AISI 316L substrates revealed substantially higher polarization resistance (R_p) due to their lower corrosion current density (I_{corr}) than AISI 316L. The coating layer provided corrosion protection to metallic substrates by acting as a barrier against electron and ions diffusion, which reduced the electrochemical reactions at the interface of 316LSS and electrolyte. In other words, due to formation of densely packed and crack-free coating (Fig. 2), nanocomposite coated samples revealed enhanced corrosion resistance compared to uncoated AISI 316L and gelatin coated substrates. The transfer resistance (Rp) of G-1F reached a value as high as 160 kV cm^2, an increase of more than 40 times compared to the Rp of the gelatin coated sample. This data further confirmed that the presence of both forsterite and gelatin could substantially enhance the corrosion resistance of AISI 316L substrates.

Furthermore, Bode plots of EIS data for the uncoated as well as pure gelatin and gelatin-forsterite coated AISI 316L substrates in PBS at pH = 7.4 are shown in Fig. 6(b). Generally, in Bode plots, higher impedance modulus (Z) at lower frequency indicated better corrosion resistance. According to Bode plots, impedance modulus (Z) of nanocomposite coated samples were higher than that of the pure gelatin coated AISI 316L which could further confirm the effective role of forsterite nanopowder on the improved dielectric behavior of gelatin coating. Moreover, similar to previous result, G-1F coated sample revealed the highest impedance modulus confirming the best corrosion resistance.

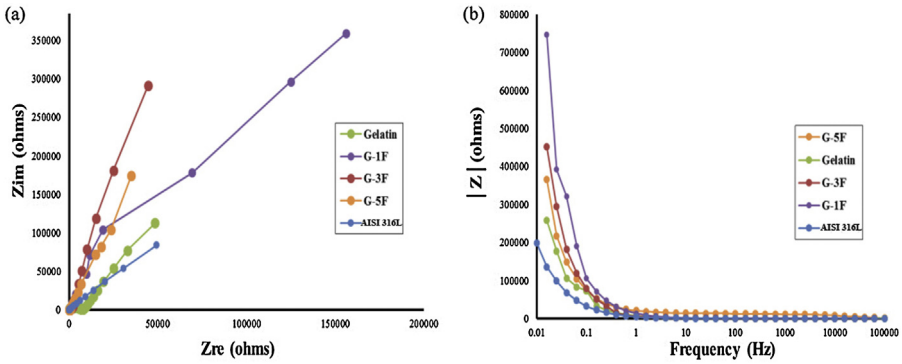

Fig. 6. (a) Nyquist and (b) Bode plots of uncoated as well as gelatin and gelatin-forsterite coated AISI 316L substrate in PBS at pH = 7.4.

4. Conclusion

In conclusion, novel nanocomposite gelatin-forsterite coatings with different amounts of forsterite nanopowder were successfully prepared on AISI 316L substrates using dip coating process and characterized regarding microstructure, coating adhesion, roughness, bioactivity and corrosion resistance. Results confirmed the formation of uniform and crack-free coatings without any defect. Forsterite nanopowder incorporated gelatin matrix could effectively improve the surface bioactivity of the samples. Moreover, increasing forsterite nanopowder significantly improved the coating adhesion and roughness compared to uncoated sample. Furthermore, potentiodynamic polarization and electrochemical impedance spectroscopy tests demonstrated superior corrosion resistance of the nanocomposite coated samples compared to uncoated and gelatin-coated substrates. To conclude, nanocomposite gelatin-forsterite coating could be suggested as a novel bioactive and corrosion resistant layer for bone implant application.

Acknowledgment

The authors are grateful for support of this research by Isfahan University of Technology.

References

[1] J. Pellier, J. Geringer, B. Forest, Fretting-corrosion between 316L SS and PMMA: influence of ionic strength, protein and electrochemical conditions on material wear. Application to orthopaedic implants, Wear 271 (9) (2011) 1563–1571.
[2] R. Suresh, P. Shruthi, R.S. Kumar, J. Siva, M.P. Ananth, R. Ramesh, Experimental investigation of nano-composite coated stainless steel (316L) surfaces under unidirectional sliding, Appl. Mech. Mater. 440 (2014) 37–41.
[3] S. Sutha, K. Kavitha, G. Karunakaran, V. Rajendran, In-vitro bioactivity, biocorrosion and antibacterial activity of silicon integrated hydroxyapatite/chitosan composite coating on 316L stainless steel implants, Mater. Sci. Eng.: C 33 (7) (2013) 4046–4054.
[4] M.B. González, S.B. Saidman, Electrodeposition of polypyrrole on 316L stainless steel for corrosion prevention, Corros. Sci. 53 (1) (2011) 276–282.
[5] V.S. Dhandapani, R. Subbiah, E. Thangavel, M. Arumugam, K. Park, Z.M. Gasem, V. Veeraragavan, D.E. Kim, Tribological properties: corrosion resistance and biocompatibility of magnetron sputtered titanium-amorphous carbon coatings, Appl. Surf. Sci. 371 (2016) 262–274.
[6] H. Zhao, J. Van Humbeeck, J. Sohier, I. De Scheerder, Electrochemical polishing of 316L stainless steel slotted tube coronary stents, J. Mater. Sci. 13 (10) (2002) 911–916.
[7] K. Zhang, J. Zou, T. Grosdidier, C. Dong, D. Yang, Improved pitting corrosion resistance of AISI 316L stainless steel treated by high current pulsed electron beam, Surf. Coat. Technol. 201 (3) (2006) 1393–1400.
[8] M. Samandi, B.A. Shedden, D.I. Smith, G.A. Collins, R. Hutchings, J. Tendys, Microstructure, corrosion and tribological behaviour of plasma immersion ion-implanted austenitic stainless steel, Surf. Coat. Technol. 59 (1) (1993) 261–266.
[9] E.W. Zhang, Y.B. Wang, K.G. Shuai, F. Gao, Y.J. Bai, Y. Cheng, X.L. Xiong, Y.F. Zheng, S.C. Wei, In vitro and in vivo evaluation of SLA titanium surfaces with further alkali or hydrogen peroxide and heat treatment, Biomed. Mater. 6 (2) (2011) 025001.
[10] F.A.N.F. Xin, C.H.E.N. Jian, J.P. Zou, W.A.N. Qian, Z.C. Zhou, J.M. Ruan, Bone-like apatite formation on HA/316L stainless steel composite surface in simulated body fluid, Trans. Nonferrous Metals Soc. China 19 (2) (2009) 347–352.
[11] K. Pardun, L. Treccani, E. Volkmann, P. Streckbein, C. Heiss, G.L. Destri, G. Marletta, K. Rezwan, Mixed zirconia calcium phosphate coatings for dental implants: tailoring coating stability and bioactivity potential, Mater. Sci. Eng.: C 48 (2015) 337–346.
[12] M. Akmal, M.A. Hussain, H. Ikram, T. Sattar, S. Jameel, J.Y. Kim, F.A. Khalid, J.W. Kim, In-vitro electrochemical and bioactivity evaluation of SS316L reinforced hydroxyapatite functionally graded materials fabricated for biomedical implants, Ceram. Int. 42 (3) (2016) 3855–3863.
[13] J. Degner, F. Singer, L. Cordero, A.R. Boccaccini, S. Virtanen, Electrochemical investigations of magnesium in DMEM with biodegradable polycaprolactone coating as corrosion barrier, Appl. Surf. Sci. 282 (2013) 264–270.
[14] J. Ballarre, I. Manjubala, W.H. Schreiner, J.C. Orellano, P. Fratzl, S. Ceré, Improving the osteointegration and bone–implant interface by incorporation of bioactive particles in sol–gel coatings of stainless steel implants, Acta Biomater. 6 (4) (2010) 1601–1609.
[15] K.P. Ananth, A.J. Nathanael, S.P. Jose, T.H. Oh, D. Mangalaraj, A novel silica nanotube reinforced ionic incorporated hydroxyapatite composite coating on polypyrrole coated 316L SS for implant application, Mater. Sci. Eng.: C 59 (2016) 1110–1124.
[16] X. Xiao, R. Liu, X. Tang, Electrophoretic deposition of silicon-substituted hydroxyapatite/poly (ε-caprolactone) composite coatings, J. Mater. Sci. Mater. Med. 20 (3) (2009) 691–697.
[17] X. Pang, T. Casagrande, I. Zhitomirsky, Electrophoretic deposition of hydroxyapatite–CaSiO3–chitosan composite coatings, J. Colloid Interface Sci. 330 (2) (2009) 323–329.
[18] L. Wang, C. Li, Preparation and physicochemical properties of a novel hydroxyapatite/chitosan–silk fibroin composite, Carbohydr. Polym. 68 (4) (2007) 740–745.
[19] S. Nagarajan, M. Mohana, P. Sudhagar, V. Raman, T. Nishimura, S. Kim, Y.S. Kang, N. Rajendran, Nanocomposite coatings on biomedical grade stainless steel for improved corrosion resistance and biocompatibility, ACS Appl. Mater. Interfaces 4 (10) (2012) 5134–5141.
[20] M. Mehdipour, A. Afshar, A study of the electrophoretic deposition of bioactive glass–chitosan composite coating, Ceram. Int. 38 (1) (2012) 471–476.
[21] M.F.M. Yusoff, M.R.A. Kadir, N. Iqbal, M.A. Hassan, R. Hussain, Dipcoating of poly (ε-caprolactone)/hydroxyapatite composite coating on Ti6Al4 V for enhanced corrosion protection, Surf. Coat. Technol. 245 (2014) 102–107.
[22] S. Sutha, K. Kavitha, G. Karunakaran, V. Rajendran, In-vitro bioactivity, biocorrosion and antibacterial activity of silicon integrated hydroxyapatite/chitosan composite coating on 316L stainless steel implants, Mater. Sci. Eng.: C 33 (7) (2013) 4046–4054.
[23] M. Kharaziha, M.H. Fathi, Improvement of mechanical properties and biocompatibility of forsterite bioceramic addressed to bone tissue engineering materials, J. Mech. Behav. Biomed. Mater. 3 (7) (2010) 530–537.
[24] G. Furtos, M.A. Naghiu, H. Declercq, M. Gorea, C. Prejmerean, O. Pana, M. Tomoaia-Cotisel, Nano forsterite biocomposites for medical applications: mechanical properties and bioactivit, J. Biomed. Mater. Res. B Appl. Biomater. 104 (7) (2016) 1290–1301.
[25] M.A. Naghiu, M. Gorea, E. Mutch, F. Kristaly, M. Tomoaia-Cotisel, Forsterite nanopowder: structural characterization and biocompatibility evaluation, J. Mater. Sci. Technol. 29 (7) (2013) 628–632.
[26] M. Kharaziha, M.H. Fathi, H. Edris, N. Nourbakhsh, A. Talebi, S. Salmanizadeh, PCL-forsterite nanocomposite fibrous membranes for controlled release of dexamethasone, J. Mater. Sci.: Mater. Med. 26 (1) (2015) 1–11.
[27] M.M. Sebdani, M.H. Fathi, Preparation and characterization of hydroxyapatite–forsterite–bioactive glass nanocomposite coatings for biomedical applications, Ceram. Int. 38 (2) (2012) 1325–1330.
[28] R. Emadi, F. Tavangarian, S.I.R. Esfahani, A. Sheikhhosseini, M. Kharaziha, Nanostructured forsterite coating strengthens porous hydroxyapatite for bone tissue engineering, J. Am. Ceram. Soc. 93 (9) (2010) 2679–2683.
[29] M.M. Sebdani, M.H. Fathi, Novel hydroxyapatite–forsterite–bioglass nanocomposite coatings with improved mechanical properties, J. Alloys Compd. 509 (5) (2011) 2273–2276.
[30] M. Kheirkhah, M. Fathi, H.R. Salimijazi, M. Razavi, Surface modification of stainless steel implants using nanostructured forsterite (Mg_2SiO_4) coating for biomaterial applications, Surf. Coat. Technol. 276 (2015) 580–586.
[31] A. Olad, F.F. Azhar, The synergetic effect of bioactive ceramic and nanoclay on the properties of chitosan–gelatin/nanohydroxyapatite–montmorillonite scaffold for bone tissue engineering, Ceram. Int. 40 (7) (2014) 10061–10072.
[32] M. Kharaziha, M.H. Fathi, H. Edris, Tunable cellular interactions and physical properties of nanofibrous PCL-forsterite: gelatin scaffold through sequential electrospinning, Compos. Sci. Technol. 87 (2013) 182–188.
[33] K.B. Djagny, Z. Wang, S. Xu, Gelatin: a valuable protein for food and pharmaceutical industries: review, Crit. Rev. Food Sci. Nutr. 41 (6) (2001) 481–492.
[34] A.A. Karim, R. Bhat, Gelatin alternatives for the food industry: recent developments, challenges and prospects, Trends Food Sci. Technol. 19 (12) (2008) 644–656.
[35] F. Frajkorová, E. Molero, B. Ferrari, Electrophoretic deposition of gelatin/hydroxyapatite composite coatings onto a stainless steel substrate, Key Eng. Mater. 654 (2015) 195–199.
[36] X. Xu, P. Lu, M. Guo, M. Fang, Cross-linked gelatin/nanoparticles composite coating on micro-arc oxidation film for corrosion and drug release, Appl. Surf. Sci. 256 (8) (2010) 2367–2371.
[37] M. Kharaziha, M.H. Fathi, Synthesis and characterization of bioactive forsterite nanopowder, Ceram. Int. 35 (6) (2009) 2449–2454.
[38] A. Saberi, B. Alinejad, Z. Negahdari, F. Kazemi, A. Almasi, A novel method to low temperature synthesis of nanocrystalline forsterite, Mater. Res. Bull. 42 (4) (2007) 666–673.
[39] Z. Chen, K. Zhou, X. Lu, Y.C. Lam, A review on the mechanical methods for evaluating coating adhesion, Acta Mech. 225 (2) (2014) 431–452.
[40] T. Kokubo, H. Takadama, How useful is SBF in predicting in vivo bone bioactivity? Biomaterials 27 (15) (2006) 2907–2915.
[41] C.J. Brinker, G.C. Frye, A.J. Hurd, C.S. Ashley, Fundamentals of sol-gel dip coating, Thin Solid Films 201 (1) (1991) 97–108.
[42] M. Park, J.E. Lee, C.G. Park, S.H. Lee, H.K. Seok, Y.B. Choy, Polycaprolactone coating with varying thicknesses for controlled corrosion of magnesium, J. Coat. Technol. Res. 10 (5) (2013) 695–706.
[43] G. Kim, J. Son, S. Park, W. Kim, Hybrid process for fabricating 3D hierarchical scaffolds combining rapid prototyping and electrospinning, Macromol. Rapid Commun. 29 (19) (2008) 1577–1581.
[44] M. Kharaziha, M. Nikkhah, S.R. Shin, N. Annabi, N. Masoumi, A.K. Gaharwar, G. Camci-Unal, A. Khademhosseini, PGS: Gelatin nanofibrous scaffolds with

tunable mechanical and structural properties for engineering cardiac tissues, Biomaterials 34 (27) (2013) 6355–6366.
[45] C.C. Mohan, A. Prabhath, A.M. Cherian, S. Vadukumpully, S.V. Nair, K. Chennazhi, D. Menon, Nanotextured stainless steel for improved corrosion resistance and biological response in coronary stenting, Nanoscale 7 (2) (2015) 832–841.
[46] M. Peter, N.S. Binulal, S.V. Nair, N. Selvamurugan, H. Tamura, R. Jayakumar, Novel biodegradable chitosan–gelatin/nano-bioactive glass ceramic composite scaffolds for alveolar bone tissue engineering, Chem. Eng. J. 158 (2) (2010) 353–361.
[47] S. Gautam, A.K. Dinda, N.C. Mishra, Fabrication and characterization of PCL/gelatin composite nanofibrous scaffold for tissue engineering applications by electrospinning method, Mater. Sci. Eng.: C 33 (3) (2013) 1228–1235.
[48] Y. Yan, X. Zhang, H. Mao, Y. Huang, Q. Ding, X. Pang, Hydroxyapatite/gelatin functionalized graphene oxide composite coatings deposited on TiO_2 nanotube by electrochemical deposition for biomedical applications, Appl. Surf. Sci. 329 (2015) 76–82.
[49] D.D. Deligianni, N.D. Katsala, P.G. Koutsoukos, Y.F. Missirlis, Effect of surface roughness of hydroxyapatite on human bone marrow cell adhesion, proliferation, differentiation and detachment strength, Biomaterials 22 (1) (2000) 87–96.
[50] T.J. Webster, R.W. Siegel, R. Bizios, Osteoblast adhesion on nanophase ceramics, Biomaterials 20 (13) (1999) 1221–1227.
[51] D.D. Deligianni, N. Katsala, S. Ladas, D. Sotiropoulou, J. Amedee, Y.F. Missirlis, Effect of surface roughness of the titanium alloy Ti–6Al–4 V on human bone marrow cell response and on protein adsorption, Biomaterials 22 (11) (2001) 1241–1251.
[52] S. Kay, A. Thapa, K.M. Haberstroh, T.J. Webster, Nanostructured polymer/nanophase ceramic composites enhance osteoblast and chondrocyte adhesion, Tissue Eng. 8 (5) (2002) 753–761.
[53] A. Balamurugan, G. Balossier, S. Kannan, S. Rajeswari, Elaboration of sol–gel derived apatite films on surgical grade stainless steel for biomedical applications, Mater. Lett. 60 (17) (2006) 2288–2293.
[54] J.W. Park, K.B. Park, J.Y. Suh, Effects of calcium ion incorporation on bone healing of Ti6Al4 V alloy implants in rabbit tibiae, Biomaterials 28 (2007) 3306–3313.
[55] S. Rammelt, T. Illert, S. Bierbaum, D. Scharnweber, H. Zwipp, W. Schneiders, Coating of titanium implants with collagen: RGD peptide and chondroitin sulfate, Biomaterials 27 (2006) 5561–5571.
[56] M. Jokar, S. Darvishi, R. Torkaman, M. Kharaziha, M. Karbasi, Corrosion and bioactivity evaluation of nanocomposite PCL-forsterite coating applied on 316L stainless steel, Surf. Coat. Technol. 307 (2016) 324–331.
[57] T. Albrektsson, C. Johansson, Osteoinduction, osteoconduction and osseointegration, Eur. Spine J. 10 (2001) S96–S101.
[58] M. Diba, M. Kharaziha, M. Fathi, M. Gholipourmalekabadi, A. Samadikuchaksaraei, Preparation and characterization of polycaprolactone/forsterite nanocomposite porous scaffolds designed for bone tissue regeneration, Compos. Sci. Technol. 72 (2012) 716–723.
[59] D. Mohn, C. Bruhin, N. Luechinger, W. Stark, T. Imfeld, T. Zehnder, Zehnder Composites made of flame-sprayed bioactive glass 45S5 and polymers: bioactivity and immediate sealing properties, Int. Endod. J. 43 (2010) 1037–1046.
[60] Y. Hosseini, R. Emadi, M. Kharaziha, A. Doostmohammadi, Reinforcement of electrospun poly (ε-caprolactone) scaffold using diopside nanopowder to promote biological and physical properties, J. Appl. Polym. Sci. (2016), Article in press.
[61] M. Eilbagi, R. Emadi, K. Raeissi, M. Kharaziha, A. Valiani, Mechanical and cytotoxicity evaluation of nanostructured hydroxyapatite-bredigite scaffolds for bone regeneration? Mater. Sci. Eng.: C 68 (2016) (2016) 603–612.
[62] C. Du, G.J. Meijer, C. Van de Valk, R.E. Haan, J.M. Bezemer, S.C. Hesseling, F.Z. Cui, K. De Groot, P. Layrolle, Bone growth in biomimetic apatite coated porous Polyactive® 1000PEGT70PBT30 implants, Biomaterials 23 (23) (2002) 4649–4656.
[63] A. Oyane, M. Kakehata, I. Sakamaki, A. Pyatenko, H. Yashiro, A. Ito, K. Torizuka, Biomimetic apatite coating on yttria-stabilized tetragonal zirconia utilizing femtosecond laser surface processing, Surf. Coat. Technol. 296 (2016) 88–95.
[64] K. Sasaki, G.T. Burstein, The generation of surface roughness during slurry erosion-corrosion and its effect on the pitting potential, Corrosion Sci. 38 (12) (1996) 2111–2120.
[65] W. Li, D.Y. Li, Influence of surface morphology on corrosion and electronic behavior, Acta Mater. 54 (2) (2006) 445–452.